Branching Ratio and Pressure Dependent Rate Constants of Multichannel Unimolecular Decomposition of Gas-Phase α-HMX: An Ab Initio Dynamics Study†

Shaowen Zhang and Thanh N. Truong*

Henry Eyring Center for Theoretical Chemistry, Department of Chemistry, University of Utah, 315 S 1400 E, Room 2020, Salt Lake City, Utah 84112

Received: November 28, 2000; In Final Form: January 17, 2001

The dynamics of the initial thermal decomposition step of gas-phase α-HMX is investigated using the master equation method. Both the NO_2 fission and HONO elimination channels were considered. The structures, energies, and Hessian information along the minimum energy paths (MEP) of these two channels were calculated at the B3LYP/cc-pVDZ level of theory. Thermal rate constants at the high-pressure limit were calculated using the canonical variational transition state theory (CVT), microcanonical variational transition state theory (μVT). The pressure-dependent multichannel rate constants and the branching ratio were calculated using the master equation method. Quantum tunneling effects in the HONO elimination are included in the dynamical calculations and found to be important at low temperatures. At the high-pressure limit, the NO_2 fission channel is found to be dominant in the temperature range (500−1500 K). Both channels exhibit strong pressure dependence at high temperatures. Both reach the high-pressure limits at low temperatures. We found that the HONO elimination channel can compete with the NO_2 fission, one in the low-pressure and/or high-temperature regime.

1. Introduction

Decomposition of energetic nitramines (HMX (octahydro-1,3,5,7-tetranitro- 1,3,5,7-tetrazocine), RDX (1,3,5-trinitro-hexahydro-s-triazine), etc.) are very complicated processes that have shown to involve hundreds of elementary reactions.[1,2] Accurate kinetic parameters of these reactions are important for modeling these complex processes in combustion and explosion. However, due to the energetic nature of these materials and the rapid rates of the intermediate reactions, it is difficult to monitor these individual reactions experimentally. Theoretical methods, especially accurate ab initio direct dynamics method ,provide a viable alternative to study the dynamics of these reactions.

Experimental studies have shown that the initial decomposition step of gas-phase HMX and RDX involves at least three possible paths:[2−6] the NO_2 fission, HONO elimination, and concerted ring fission paths. Since the ring fission reaction has much higher activation energy, the NO_2 fission and HONO elimination channels are energetically more favorable. Previous experimental results revealed that NO_2 fission is the dominant path at low temperatures for gas-phase HMX.[4,7] It is very interesting to note that theoretical study on the mechanism and kinetics of thermal decomposition of gas-phase HMX has been rather limited. There have been several theoretical studies on the mechanism, particularly the initial decomposition steps, of the smaller RDX.[8−11] Thermal rate constants for the NO_2 fission channel of RDX have also been estimated by the simple TST method.[2] Yetter and co-workers have proposed a rather detailed mechanism consisting of 256 reactions for the decomposition of RDX.[1] In this mechanism, the HONO elimination channel was not included for the reason mentioned above. A recent theoretical study on the decomposition mechanism of RDX showed that the barrier for the HONO elimination is only 0.2 kcal/mol higher than that of the NO_2 fission.[11] Although these results are subjected to uncertainty in the level of theory and basis set used, they suggested that the contribution from the HONO elimination channel might not be negligible. In fact, the HONO elimination channel might even be faster than the NO_2 fission channel for RDX at low temperatures due to possible quantum-tunneling effects from the motion of the light hydrogen atom. To the best of our knowledge, there has not been any dynamical study on the relative importance of these channels and tunneling effects in the HONO elimination channel either for the gas-phase RDX or HMX.

It is our long-term goal to provide a detailed mechanism with associated kinetic parameters for the decomposition of the gas-phase HMX. Our initial progress in this direction was the recent kinetic study[12] of the NO_2 fission of HMX from first principles. The direct ab initio dynamics approach was utilized where rate constants were calculated from the microcanonical variational transition state theory using potential energy surface information from an accurate hybrid nonlocal density functional theory. The calculated rate constants were in excellent agreement with available experimental data at low temperatures. This is an encouraging sign. However, as mentioned earlier, the initial decomposition of gas-phase HMX or RDX has a multichannel nature. As discussed above, the HONO elimination channel may compete with the NO_2 bond fission channel. Furthermore, unimolecular decomposition reactions often exhibit strong pressure dependence. Such dependence has not been addressed either for the decomposition of gas-phase RDX or HMX. Thus, it is important to provide rate constants as well as the branching ratio of these two channels as functions of both the temperature and pressure. The multichannel dynamics and pressure-dependent rate constants can be studied using the well-developed master equation (ME) method.[13−19] This method has been employed in many recently theoretical studies[18,20−28] on the pressure dependent rate constants. The ME method requires the microcanonical rate constants, $k(E)$, for each channel. The constant

† Part of the special issue "Aron Kuppermann Festschrift".

10.1021/jp0043064 CCC: $20.00
Published on Web 02/15/2001

$k(E)$ can be calculated from either the variational or conventional microcanonical transition state theory (μVT or μTST, respectively).[29−31] To obtain an accurate branching ratio, tunneling effects in the HONO elimination step should be included in rate calculations. This gives a new challenge to the dynamical methodology because such inclusion has not been done in most applications of the theory. Miller proposed an approach for inclusion of tunneling effects in $k(E)$ using an one-dimensional Eckart tunneling model, though it has not been widely employed in actual applications due to its large computational demand.[32]

In this study, we present a direct ab initio dynamics study on the branching ratio and pressure-dependent rate constants for the decomposition of gas-phase α-HMX using the ME method coupled with the microcanonical variational transition state theory. Both the NO_2 bond fission and HONO elimination channels are considered.

2. Methodology

2.1. Rate Constants Calculations. Both canonical variational transition state theory[33,34] (CVT) and microcanonical variational transition state theory[30,35] (μVT) were employed to calculate the high-pressure limit thermal rate constants for both NO_2 fission and HONO elimination reactions. The multichannel and pressure-dependent rate constants were calculated by using the master equation (ME) method.[13−17] Quantum tunneling effects were included in the rate constant calculations of the HONO elimination reaction by using the small curvature tunneling[36,37] (SCT) method in the CVT framework and Miller's one-dimensional Eckart tunneling model[32] in the μVT framework. There is considerable literature on the CVT, μVT, and SCT methods,[29−31] thus we will not discuss them here. Below we give only some details for our implementation of Miller's tunneling model in the microcanonical TST framework and a brief overview of the master equation method for calculations of multichannel rate constants. These methods have been implemented in the TheRate program.[38]

2.1.1. Quantum Tunneling Effects in Microcanonical Rate Constants. The microcanonical rate constant for a unimolecular reaction at fixed energy E is given by[19,30]

$$k(E) = \frac{N^{\neq}(E)}{h\rho(E)} \tag{1}$$

where $N^{\neq}(E)$ is the sum of states at the transition state, $\rho(E)$ is the density of states at the reactant, and h is Plank's constant. In Miller's one-dimensional tunneling model, $N^{\neq}(E)$ can be expressed as a sum of one-dimensional tunneling probabilities[32]

$$N^{\neq}(E) = \sum_n P(E - E_n^{\neq}) \tag{2}$$

where n is the subscript of the microstates of the transition state; $E_n^{\neq}$ is the energy distributed in microstate n of the transition state, and $P(E - E_n^{\neq})$ is the quantum tunneling probability with respect to microstate n. Within the symmetrical-top rigid rotor and harmonic oscillator approximations, eq 2 becomes

$$N^{\neq}(E) = \sum_{J=0}^{J_{max}} \sum_{K=-J}^{J} \sum_m P(E - V_0 - E_{J,K}^{\neq} - E_m^{\neq}) \tag{3}$$

where J and K are quantum numbers of rotational angular momentum; J_{max} is the maximum available value of J; m is a set of vibrational quantum numbers at the transition state ($m = (m_1, m_2, ..., m_{Nvib})$; N_{vib} is the number of real vibrational frequencies); V_0 is the classical barrier height; $E_{J,K}^{\neq}$ is the rotational energy at the quantum state (J, K); $E_m^{\neq}$ is the vibrational energy corresponding to the set of quantum numbers m. The tunneling probability $P(E - V_0 - E_{J,K}^{\neq} - E_m^{\neq})$ has the analytical expression for a one-dimensional Eckart potential.[32] Equation 3 can be computationally demanding for large molecules because it involves summations of all possible rotational and vibrational quantum states J, K, and m.

In this study we have modified the Beyer and Swinehart method to include quantum-tunneling effects. The Beyer and Swinehart method is a very efficient algorithm[39,40] to calculate sum and density of states for vibrational modes. In this method, instead of looping over all of the quantum numbers of each vibrational mode, only two loops, one over energies and the other over the number of vibrational modes, are required. Another advantage of the Beyer−Swinehart method is that when $N^{\neq}(E)$ and $\rho(E)$ are evaluated at a given E, their values at lower energies are also computed. Thus, one needs only to calculate $N^{\neq}(E)$ and $\rho(E)$ once at $E = E_{max}$. More details of the Beyer−Swinehart method can be found elsewhere.[39,40] Within the Beyer−Swinehart framework, eq 3 has the form

$$N^{\neq}(E) = \sum_{J=0}^{J_{max}} \sum_{K=-J}^{J} \sum_{E_V=0}^{E-V_0-E_{J,K}^{\neq}} (\rho(E_V)\Delta E_V) P(E - V_0 - E_{J,K}^{\neq} - E_V) \tag{4}$$

where E_V is the energy distributed in vibrational motions; $\rho(E_V)$ is the density of vibrational states at energy E_V; ΔE_V is the energy increment. Notice that the loop over the vibrational modes in eq 3 is replaced by the loop of energy in eq 4. The upper bounds of the three loops in eq 4 are determined by the energy E (J_{max} is also determined by E).

Equation 4 is still computationally demanding, particularly for large molecules due to the loops over J and K quantum numbers. For large molecules such as HMX, J_{max} can be larger than 3000 at the excess energy of about 340 kcal/mol in our calculations. However, for large molecules where rotational constants are rather small, the rotational energy varies very slowly with K. In such cases, we can approximate the contribution to the sum over K in eq 4 for J larger than a specific J_s value by

$$N^{\neq}(E) = \sum_{J=J_s}^{J_{max}} (2J+1) \sum_{E_V=0}^{E-V_0-E_J^{\neq}} (\rho(E_V)\Delta E_V) P(E - V_0 - \bar{E}_J^{\neq} - E_V) \tag{5}$$

The average energy $\bar{E}_J^{\neq}$ is calculated from averaging $E_{J,K}^{\neq}$ at several values of K for a given J. In actual calculations of HMX, we found that for $J_s = 20$ and the average energy $\bar{E}_J^{\neq}$ calculated from nine uniform grid points from 0 to J, about 3% error in the calculated rate constant was introduced. However, the gain in the computational efficiency is by several orders of magnitude, particularly for large molecules such as HMX. Such an approximation does need further examination for other systems.

2.1.2. Pressure-Dependent Multichannel Rate Constants. The master equation method can be formulated in the discrete form for a multichannel unimolecular reaction as follows[19]

$$\frac{dP_i}{dt} = \omega \sum_j (R_{ij}P_j - R_{ji}P_i) - \sum_m k_i^m P_i \tag{6}$$

where ω is the collision frequency of the reactant molecules with bath gas; P_i is the population of the activated reactant at the energy level i; R_{ij} is the collision induced transition rate of reactant from the energy level j to i; k_i^m is the microcanonical rate constants of the channel m at the energy level i. The first term on the right-hand side of eq 6 describes the increase in the population of the reactant at the energy level i, while the remaining two terms describes the decrease in its population via collision with bath molecules and via chemical reactions, respectively. Equation 6 can be rewritten in the matrix form

$$\frac{d\mathbf{P}}{dt} = \mathbf{JP} \tag{7}$$

where **P** is a column vector with elements P_i, and the elements of matrix **J** are defined from eq 6

$$J_{ij} = \omega R_{ij} \qquad i \neq j \tag{8}$$

$$J_{ii} = -\omega \sum_{j \neq i} R_{ji} - \sum_m k_i^m \tag{9}$$

It was shown that the negative of the largest eigenvalue of matrix **J** is the thermal rate constants k_{uni}

$$\mathbf{Jg} = -k_{uni}\mathbf{g} \tag{10}$$

where **g** is the eigenvector corresponding to the largest eigenvalue k_{uni}. Because the elements of matrix **J** depend on pressure, the multichannel thermal rate constants k_{uni} in eq 10 are pressure dependent. We can calculate the rate constants for any specific channel by including only the microcanonical rate constants of that particular channel in eq 10. In our calculations, the energy transfer rate was calculated by the exponential down model,[19] and eq 10 was solved by the numerical method based on the Nesbet algorithm.[41]

2.2. Electronic Structure Calculations. Johnson et al.[42] recently reported a detailed study on the performance of different nonlocal hybrid density functional theory (DFT) methods in comparison with results of accurate quadratic configuration interaction with single and double excitations (QCISD) and with a correction for triple excitations (QCISD(T)) calculations for the NO_2 fission and HONO elimination from dimethylnitramine (DMNA). They found that all considered DFT methods (Becke's one parameter functional with the correlation functional of Lee, Yang, and Parr (B1LYP), Becke's half-and-half functional with LYP correlation functional (BH&HLYP), Barone and Adamo's Becke-style one-parameter functional with modified Perdew−Wang exchange and Perdew−Wang 91 correlation (MPW1PW91), and Becke's three-parameter functional with LYP correlation functional (B3LYP)) perform well in predicting stationary-point geometries in comparison with those from the QCISD method. For energetic information, only the B1LYP and B3LYP with the Dunning's correlation-consistent double-ξ plus polarization (cc-pVDZ) basis set[43] can predict the reaction barriers for both the NO2 and HONO elimination reactions to within 1 kcal/mol of those from the QCISD(T)//QCISD/cc-pVDZ calculations. Because the B3LYP method[44] is more widely used and tested, the B3LYP/cc-pVDZ level of theory is chosen for this study.

For the HONO elimination channel, the transition state has been verified to have only one imaginary frequency vibrational mode that connects the reactant and products. The IRC was calculated in the mass-weighted internal coordinate with the small step size of 0.02 amu$^{1/2}$ bohr using the Gonzalez−Schlegel method.[45] A total of 21 points along the IRC (intrinsic reaction coordinate) were selected for Hessian calculations by the autofocusing technique.[38] The NO_2 fission channel generates two free radicals, thus, the singlet open shell B3LYP method with a mix of the frontier molecular orbitals was adopted. Because this reaction channel has no barrier, the reaction coordinate is approximated to be the broken N−N bond distance, whereas other geometrical parameters are fully optimized. Hessian matrices at selected points along the reaction coordinated were calculated and used in μVT and CVT calculations of rate constants. All electronic structure calculations were performed using the GAUSSIAN 98 program.[46] Rate constants were calculated using the new modules of the TheRate program.[38]

3. Results and Discussion

3.1. Potential Energy Surface. Although no theoretical studies on the HONO elimination of HMX have been reported to date, there were previous calculations on the same reaction for related nitramines.[11,42] For α-HMX, because there are two different NO_2 groups, namely the axial and equatorial groups, there are two possible HONO elimination pathways. However, we found that both pathways converge to the same transition state and products via a concerted process. The concerted mechanism for this pathway is consistent with recent theoretical study[11] of the decomposition mechanism of RDX by Chakraborty et al. The calculated zero-point energy corrected barrier is 42.4 kcal/mol, that is about 3.2 kcal/mol higher than that of RDX from Chakraborty et al. calculations. A noticeable difference between the present study and that of Chakraborby et al. is that in our calculation for HMX, the barrier for the HONO elimination is about 2.7 kcal/mol higher than that of NO_2 fission reaction,[12] whereas this difference is only 0.2 kcal/mol for RDX.[11] In addition, the calculated HONO elimination transition state for HMX has a tighter structure, with the active N−N, H−C, and H−O bond distances being 1.996 Å, 1.436 Å, and 1.200 Å, respectively as compared to 2.104 Å, 1.332 Å and 1.305 Å, respectively for RDX.[11] This could be due to the differences in reactivity of the two species. It could also be attributed to the difference in the basis sets used in these two calculations, namely the cc-pVDZ basis set in our calculations versus the 6-31G(d) in the previous study for RDX. Note that the cc-pVDZ includes a set of p polarization functions for hydrogen atoms and d polarization functions for second-row atoms, whereas polarization functions for hydrogen atom are not included in the 6-31G(d) basis set. In the previous study[42] for DMNA, it was shown that the B3LYP/cc-pVDZ level is more accurate than the B3LYP/6−31 g(d) level for predicting transition state properties in comparison to the QCISD/cc-pVDZ level of theory.

Potential energy along the IRC of the HONO elimination channel is shown in Figure 2. Figure 3 depicts variations of selected bond lengths, particularly the active N−N, C−H, and C−O bonds along the reaction coordinate. In the range of the reaction coordinate from −1.0 to +1.0, the active C−H bond changes from 1.12 Å (about 10% longer than its equilibrium value) to 1.72 Å, the H−O bond from 1.6 to 1.02 Å, while the N−N bond remains almost unchanged at around 2.0 Å (more than 40% larger than its equilibrium value). These results indicate that the HONO elimination reaction consists of three stages, namely the N−N bond elongation initially, then the hydrogen migration from the C atom to the O atom, and finally the HONO molecule cleavage. The first stage accounts for at least 74% of the barrier, i.e., 35 kcal/mol, whereas the hydrogen migration requires the remaining 12 kcal/mol of the barrier.

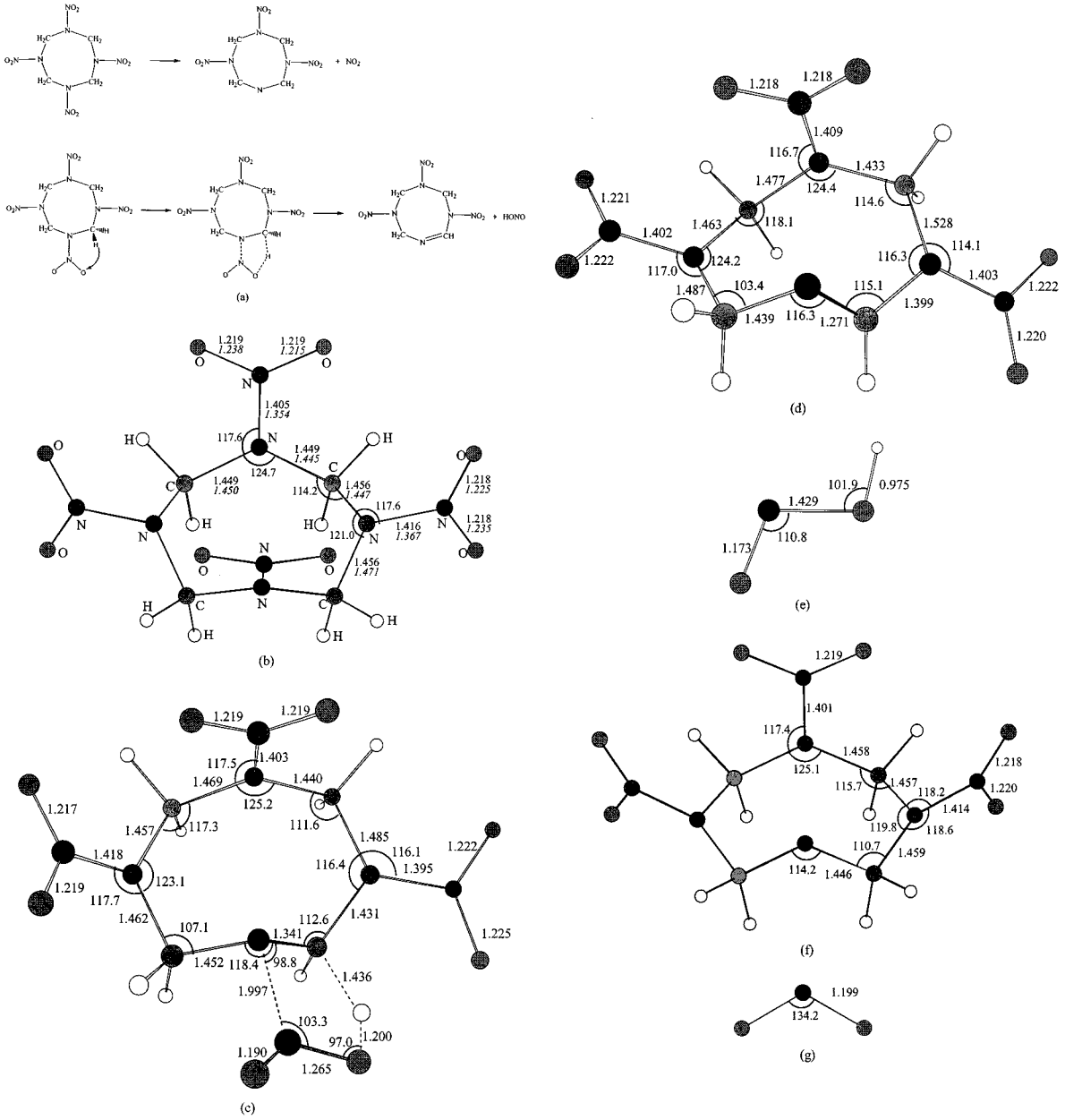

Figure 1. (a) Schematic diagram of the NO_2 fission and HONO elimination channels of α-HMX. (b) Optimized geometry of α-HMX. (c) Optimized geometry of the transition state of the HONO elimination channel. (d) and (e) Optimized geometries of the products of the HONO elimination channel. (f) and (g) Optimized geometries of the products of the NO_2 fission channel.

Thus, only the top part of the potential barrier is important in tunneling calculations and potential energy information along the MEP for the absolute value of the reaction coordinate greater than 1.0 is not critical for the dynamics and is not needed.

The NO_2 fission channel is found to be an endothermic process without barrier. The similarity in the geometries of the reactant HMX (Figure 1b) and of the products (Figure 1f) supports the use of the broken N−N bond length as the reaction coordinate. We found that the axial and equatorial NO_2 fission pathways become degenerate after the N−N bond length longer than 2.7 Å. The calculated reaction energy is 44.17 kcal/mol. Including the zero-point-energy correction, it reduces to 39.73 kcal/mol. The potential energy profile becomes flat as the breaking N−N bond length is larger than 2.5 Å, i.e., the energy rises only 3.79 kcal/mol in the range from 2.5 Å to 3.5 Å. This region is particular important for the variational transition state calculations. The energy profile for the NO_2 fission reaction is given in Figure 4.

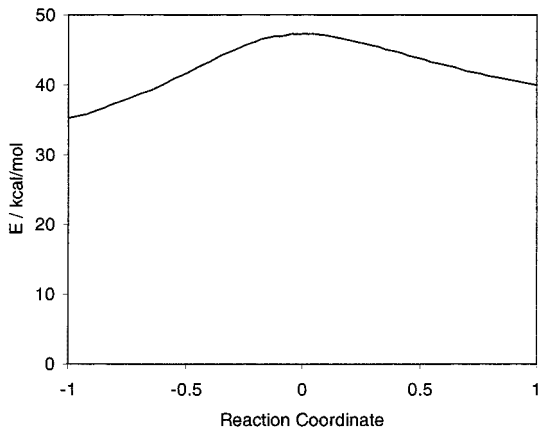

Figure 2. Plot of the potential energy along the minimum energy path of the HONO elimination channel.

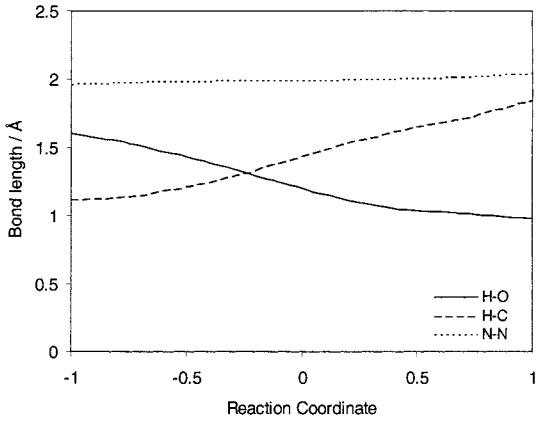

Figure 3. Variations of selected bond lengths along the minimum energy path of the HONO elimination channel.

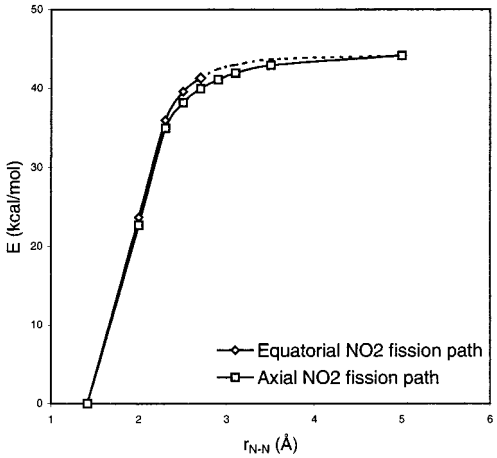

Figure 4. Plot of the potential energy profile vs the breaking N−N bond length of the NO_2 fission channel.

3.2. Rate Constants at the High-Pressure Limit. We employed both CVT[33,34] and μVT[19,30,35] methods to calculate the thermal rate constants at the high-pressure limit. Tunneling effects for the HONO elimination channel are calculated using the SCT method[36] in CVT calculations and Miller's Eckart tunneling method[32] in μVT calculations. The calculated rate constants for both the NO_2 and HONO elimination channels are depicted in Figure 5 together with available experimental data[47−50] for the NO_2 fission channel (unfortunately, experimental data for the HONO elimination channel is currently not available). In the present rate calculations, we used the statistical factors 4 for the NO_2 fission reaction because the four NO_2 fission paths degenerated as mentioned earlier. The statistical factor for the HONO elimination reaction is 8 because each NO_2 has two oxygen atoms that can react only with the nearest hydrogen atom of the methylene group (the other hydrogen atom in the same methylene group is too far for feasible migration). First of all, the calculated rate constants of the NO_2 bond fission channel are within the uncertainty of the available experimental data at low temperatures. The experimental data[47−50], however, are rather scattered and located mainly at very low temperatures due to differences in experimental conditions and explosive nature of HMX. It can be seen that within the temperature range from 250 to 1500 K, the HONO elimination rate constants are noticeably smaller than that of the other channel. The temperature and pressure dependence of the branching ratio of these two channels is discussed separately below. We found that tunneling effects are important in the HONO elimination, particularly at low temperatures. At 250 K, tunneling is predicted

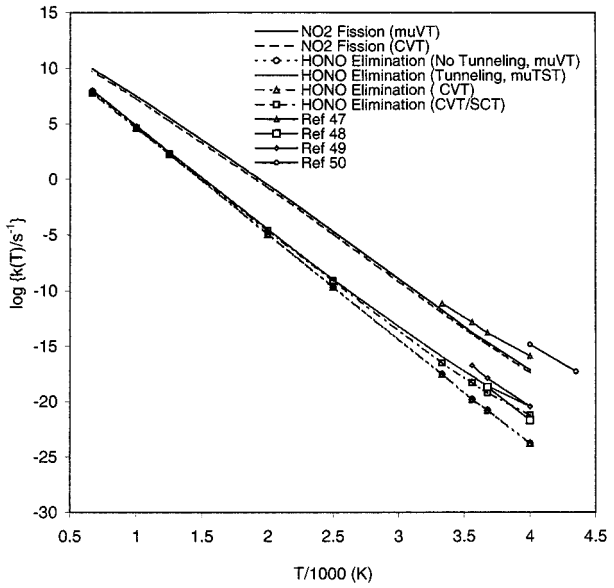

Figure 5. Plot of the thermal rate constants at the high-pressure limits vs temperature. Solid lines with symbols are the experimental data for the NO_2 bond fission channel. Note CVT and μVT (without tunneling) results are almost identical for HONO elimination reaction.

to enhance the HONO elimination rate by a factor of 350 using the CVT/SCT method and 2089 using the μVT/Eckart method. As expected, the tunneling effects decrease as the temperature increases. The difference in the tunneling contribution calculated from these two methods could be due to combinations of several factors. One is the width of the Eckart function being too narrow, thus overestimating the tunneling probability. However, the Eckart model does not include the "corner cutting", i.e., reaction path curvature effects, as included in the SCT method. The other is that the mVT methodology includes tunneling for all possible vibrational and rotational states, whereas the SCT method assumes all vibrational modes are in the ground state and no contributions from the rotational motions. However, since the HONO elimination has rather a substantial barrier, we believe that the large transmission coefficient calculated from the μVT/Eckart method as compared to the CVT/SCT method is due mainly to contributions from the vibrational excited states of HMX.

It is interesting to note that both CVT and μVT methods predict nearly identical thermal rate constants for both channels. When including tunneling effects, CVT/SCT and μVT/Eckart results for the HONO elimination channel differ somewhat. Particularly, the μVT/Eckart rate constant is larger by a factor of 6 at 250 K. Overall, the differences are acceptably small between the two methods. These results support the use of the CVT/SCT method in future calculations of thermal rate constants. The μVT/Eckart method is much more computationally demanding and thus should be employed only when pressure-dependent rate constants are needed.

3.3. Pressure Dependent Multichannel Rate Constants. In calculations of the pressure-dependent rate constants of both NO_2 fission and HONO elimination channels, argon was used as the bath gas to compute the collision frequency using the Lennard-Jones model with σ and ϵ parameters of 7.1 Å and 794.0 K, respectively. These parameters were estimated by the method of Reid et al.[51] The typical energy grain of 100 cm^{-1} was selected. Test calculations showed that reducing the energy grain to 50 cm^{-1} does not noticeably change the final results. Rate constants were calculated at three different energy transfer values: 300, 800, and 1500 cm^{-1} in order to provide estimation

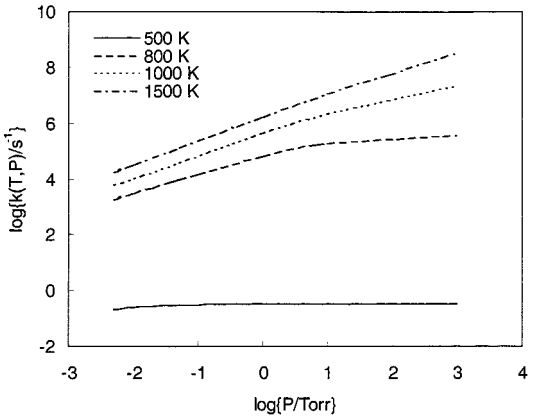

Figure 6. Plot of the pressure-dependent rate constants of the NO_2 fission channel at the energy transfer value of 800 cm^{-1}.

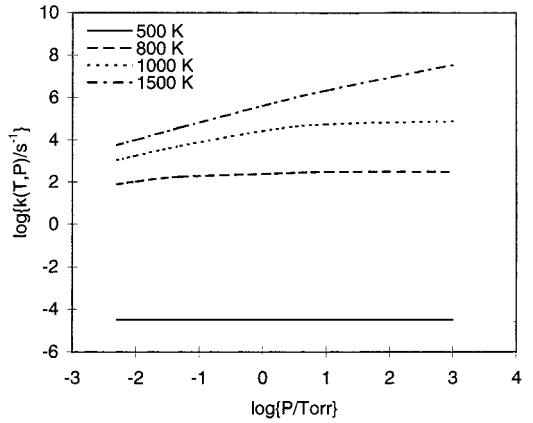

Figure 7. Plot of the pressure-dependent rate constants of the HONO elimination channel at the energy transfer value of 800 cm^{-1}.

of rate constants from the weak to strong collision conditions. The dependence of rate constants on the energy transfer parameter is discussed below in a separate subsection. For the discussion of the pressure dependence of the rate constants and of the branching ratio, we used the results from the intermediate energy transfer parameter of 800 cm^{-1}.

Figures 6 and 7 show the pressure-dependent rate constants for the NO_2 fission channel and HONO elimination channel, respectively. The rate constants for both channels exhibit very weak dependence on the pressure at 500 K. The pressure dependence becomes more profound as the temperature increases. At 1500 K, both reactions show strong pressure dependence, even at normal pressure (760 Torr). Particularly, at normal pressure the rate constants of the NO_2 and HONO elimination channels are smaller than their high-pressure limits by factors of 33.4 and 3.77, respectively. This phenomenon can be easily explained by the strong collision model, in which the pressure dependent-rate constant is given by[19]

$$k_{\text{uni}} = \int_{E_0}^{\infty} f(E)k(E)\frac{Z[M]}{Z[M] + k(E)} \qquad (11)$$

where $f(E)$ is the distribution function; Z is the collision number; $[M]$ is the concentration of bath gas; $k(E)$ are the microcanonical rate constants. In eq 11, $[M]$ is the only part that relates to the pressure. At the high-pressure limit, $Z[M] \gg k(E)$, $k(E)$ can be omitted and k_{uni} is independent of the pressure. Here, k_{uni} can reach the high-pressure limit sooner at the lower temperature. This is because at low temperatures the Boltzmann distribution function centers at the lower energy where $k(E)$ are small, and thus the high-pressure limit condition $Z[M] \gg k(E)$ can be satisfied easily.

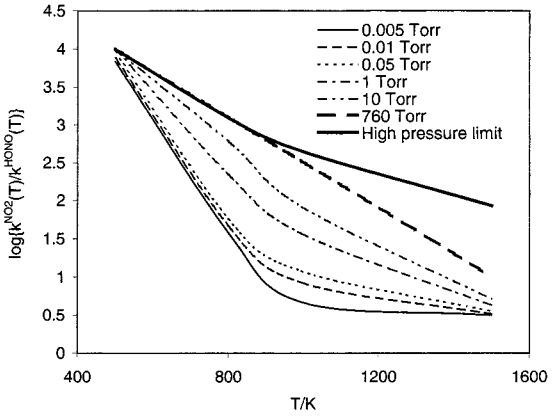

Figure 8. Plot of the branching ratio vs temperature for different pressures at the energy transfer value of 800 cm^{-1}.

The NO_2 fission reaction shows a stronger pressure dependence than the does HONO elimination reaction. At 800 K, the HONO elimination reaction is almost pressure independent in the pressure range from 5×10^{-3} to 10^3 Torr, whereas the NO_2 fission reaction reaches the falloff region when the pressure drops below 10 Torr.

3.4. Branching Ratios. Figure 8 plots of the branching ratios of rate constants of the two channels, namely k_{NO2}/k_{HONO} as functions of the temperature and pressure. It can be seen that at a given temperature the branching ratio increases with the pressure. It reaches the high-pressure limit at low temperature due to the reason discussed above. As the temperature increases, it exhibits strong pressure dependence. Particularly at the normal pressure and at the temperature of 1500 K, which is typical in combustion systems, the branching ratio is 9.55, which is much smaller than the high-pressure limit value of 84.8. It is interesting to point out that in the temperature range where experimental data are available, the branching ratio is larger by more than 4 orders of magnitude, thus the contribution of the HONO elimination channel is negligible and is consistent with the experimental observation. However, in the temperature range that is typical in combustion systems, i.e., ~1500 K, and at standard pressure, the branching ratio is only 9.55. This indicates that the contribution of the HONO elimination channel is not negligible and should be included in the kinetic model in thermal decomposition of HMX. Due to the similarity between RDX and HMX, this conclusion is also relevant for RDX.

3.5. Influence of the Energy Transfer Parameter. The energy transfer parameter is important in determining the energy transfer rate. Unfortunately, currently there is no sophisticated method to estimate this value. To show the influence of energy transfer parameter on the pressure-dependent rate constants, we calculated the rate constants at three values 300, 800, and 1500 cm^{-1} ranging from the weak to strong collision condition for both the NO_2 fission and HONO elimination channels. The results are depicted in Figures 9a and 9b, respectively. The variation between the lower and higher limits can be thought of as the maximum uncertainty in the pressure-dependent rate constants. Because the rate constants of the NO_2 bond fission channel show a stronger dependence on the pressure, it also exhibits the larger influence by the energy transfer parameter. As the pressure increases, the differences between rate constants from different values of this parameter decrease as expected. Furthermore, as the temperature increases, the variation also increases. At normal pressure and at 1500 K, the differences

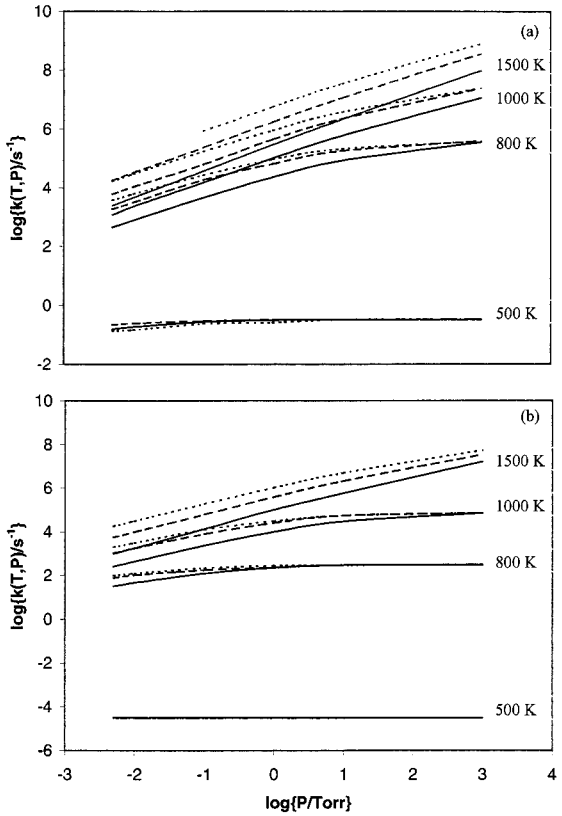

Figure 9. Influence of the energy transfer value on the pressure-dependent rate constants of the NO_2 channel (a) and HONO elimination channel (b). The dotted line is for energy transfer value of 1500 cm^{-1}; the dashed line for energy transfer value of 800 cm^{-1} and the solid line for energy transfer value of 300 cm^{-1}.

between the lower and higher energy transfer parameters is about 8.31 for the NO_2 bond fission and 3.31 for the HONO elimination channel. Thus, it does not affect the conclusions in this study.

4. Conclusions

We presented a direct ab initio dynamics study of the branching ratio and pressure-dependent rate constants of the multichannel thermal decomposition of gas-phase α-HMX. Particularly, only the initial step of the decomposition with both the NO_2 fission and HONO elimination channels was considered. The master equation was employed. Both canonical and microcanonical variational transition state (CVT and μVT) theories were carried out. Quantum mechanical tunneling effects in the HONO elimination channel were included using the multidimensional semiclassical small curvature (SCT) method in the CVT framework and the Eckart model in the μVT framework. Potential energy information was calculated at the B3LYP/cc-pVDZ level of theory.

We found that both the NO_2 bond fission and HONO elimination channels exhibit a strong pressure dependence in the temperature range that is typical in most combustion systems, i.e., $T > 1000$ K. At the normal pressure and 1500 K, the thermal rate constants of the NO_2 bond fission and HONO elimination channels are smaller than their high-pressure limits by a factor of 33.4 and 3.77, respectively. Our results are consistent with experimental observation that the contribution from the HONO elimination channel is negligible with the branching ratio k_{NO2}/k_{HONO} less than 1.0×10^4 for temperatures below 300 K, where experiments can be carried out for this energetic material. However, for temperatures that are typical in combustion systems, i.e., above 1000 K, its contribution is not negligible. Particularly, at normal pressure and 1500 K, the branching ratio is only 9.55, namely 9.5% of the total rate. In light of these results, this reaction channel should be included in the kinetic models for the thermal decomposition of HMX and RDX.

Acknowledgment. This work is supported by the University of Utah Center for the Simulation of Accidental Fires & Explosions, funded by the Department of Energy, Lawrence Livermore National Laboratory, under subcontract B341493. An allocation of computer time from the Center for High Performance Computing is gratefully acknowledged.

References and Notes

(1) Yetter, R. A.; Dryer, F. L.; Allen, M. T.; Gatto, J. L. *J. Propul. Power* **1995**, *11*, 683.
(2) Melius, C. F. Thermochemical Modeling: I. Application to Decomposition of Energetic Materials. In *Chemistry and Physics of Energetics Materials*; Bulusu, S. N., Ed.; Kluwer Academic: Dordrecht, 1990.
(3) Zhao, X.; Hinsta, E. J.; Lee, Y. T. *J. Chem. Phys.* **1988**, *88*, 801.
(4) Botcher, T. R.; Wight, C. A. *J. Phys. Chem.* **1994**, *98*, 5441.
(5) Behrens, R., Jr. *J. Phys. Chem.* **1991**, *95*, 5838.
(6) Behrens, R., Jr. *J. Phys. Chem.* **1990**, *94*, 6706.
(7) Pace, M. D. *J. Phys. Chem.* **1991**, *95*, 5858.
(8) Harris, N. J.; Lammertsma, K. *J. Am. Chem. Soc.* **1997**, *119*, 6583.
(9) Guo, Y.; Thompson, D. L. *J. Phys. Chem. B* **1999**, *103*, 10599.
(10) Wu, C. J.; Fried, L. E. *J. Phys. Chem. A* **1997**, *101*, 8675.
(11) Chakraborty, D.; Muller, R. P.; Dasgupta, S.; Goddard, W. A., III. *J. Phys. Chem. A* **2000**, *104*, 2261.
(12) Zhang, S.; Truong, N. T. *J. Phys. Chem. A* **2000**, *104*, 7304.
(13) Zwolinski, B. J.; Eyring, H. *J. Am. Chem. Soc.* **1947**, *69*, 2702.
(14) Montroll, E. W.; Shuler, K. E. *Adv. Chem. Phys.* **1958**, *1*, 361.
(15) Lin, Y. N.; Rabinovitch, B. S. *J. Phys. Chem.* **1968**, *72*, 1726.
(16) Troe, J. *J. Chem. Phys.* **1977**, *66*, 4745.
(17) Gilbert, R. G.; Luther, K.; Troe, J. *Ber. Bunsen-Ges. Phys. Chem.* **1983**, *87*, 169.
(18) Robertson, S. H.; J., P. M.; Gates, K. E.; Smith, S. C. *J. Comput. Chem.* **1997**, *18*, 1004.
(19) Gilbert, R. G.; Smith, S. C. *Theory of Unimolecular and Recombination Reactions*; Blackwell Scientific: Carlton, Australia, 1990.
(20) Blitz, M.; Pilling, M. J.; Robertson, S. H.; Seakins, P. W. *Phys. Chem. Chem. Phys.* **1999**, *1*, 73.
(21) Fahr, A.; Laufer, A. H.; Tardy, D. C. *J. Phys. Chem. A* **1999**, *103*, 8433.
(22) Klippenstein, S. J.; Harding, L. B. *J. Phys. Chem. A* **1999**, *103*, 1089.
(23) Klippenstein, S. J.; Harding, L. B. *J. Phys. Chem. A* **2000**, *104*, 2351.
(24) McIlroy, A. T., F. P. *J. Chem. Phys.* **1993**, *99*, 3597.
(25) Meyer, A.; Schroeder, J.; Troe, J. *J. Phys. Chem. A* **1999**, *103*, 10528.
(26) Pawlowska, Z.; Gardiner, W. C.; Oref, I. *J. Phys. Chem.* **1993**, *97*, 5024.
(27) Pereira, R. D. A.; Baulch, D. L.; Pilling, M. J.; Robertson, S. H.; Zeng, G. *J. Phys. Chem. A* **1997**, *101*, 9681.
(28) Smith, S. C.; Gilbert, R. G. *Int. J. Chem. Kinet.* **1988**, *20*, 979.
(29) Truhlar, D. G.; Garrett, B. C.; Klippenstein, S. J. *J. Phys. Chem.* **1996**, *100*, 1.
(30) Hase, W. *ACC. Chem. Res.* **1998**, *31*, 659.
(31) Garrett, B. C. *Theor. Chem. Acc.* **2000**, *103*, 200.
(32) Miller, W. H. *J. Am. Chem. Soc.* **1979**, *101*, 6810.
(33) Truhlar, D. G.; Garrett, B. C. *Annu. Rev. Phys. Chem.* **1984**, *35*, 159.
(34) Truhlar, D. G.; Isaacson, A. D.; Garrett, B. C. Generalized transition state theory. In *Theory of Chemical Reaction Dynamics*; Baer, M., Ed.; CRC Press: Boca Raton: Florida, 1985; Vol. 4; p 65.
(35) Truhlar, D. G.; Garrett, B. C.; Klippenstein, S. J. *J. Phys. Chem.* **1996**, *100*, 12771.
(36) Truhlar, D. G.; Isaacson, A. D.; Skodje, R. T.; Garrett, B. C. *J. Phys. Chem.* **1982**, *86*, 2252.
(37) Lu, D.-h.; Truong, T. N.; Melissas, V. S.; Lynch, G. C.; Liu, Y. P.; Garrett, B. C.; Steckler, R. I., A. D.; Rai, S. N.; Hancock, G. C.; Lauderdale, J. G.; Josepoh, T.; Truhlar, D. G. *Comput. Phys. Commun.* **1992**, *71*, 235.
(38) Duncan, W. T.; Bell, R. L.; Truong, T. N. *J. Compt. Chem.* **1998**, *19*, 1039. The program is available at http://uklab.hec.utah.edu.
(39) Stein, S. E.; Rabinovitch, B. S. *J. Phys. Chem.* **1973**, *58*, 2438.

(40) Beyer, T.; Swinehart, D. F. *Comm. Assoc. Comput. Machines* **1973**, *16*, 379.
(41) Nesbet, R. *J. Chem. Phys.* **1965**, *43*, 311.
(42) Johnson, M. A.; Truong, T. N. *J. Phys. Chem. A* **1999**, *103*, 8840.
(43) Woon, D. E.; Dunning, T. H., Jr. *J. Chem. Phys.* **1993**, *98*, 1358.
(44) Becke, A. D. *J. Chem. Phys.* **1993**, *98*, 5648.
(45) Gonzalez, C.; Schlegel, H. B. *J. Phys. Chem.* **1990**, *94*, 5523.
(46) Frisch, M. J.; Trucks, G. W.; Schlegel, H. B.; Scuseria, G. E.; Robb, M. A.; Cheeseman, J. R.; Zakrzewski, V. G.; Montgomery, J., J. A.; Stratmann, R. E.; Burant, J. C.; Dapprich, S.; Millam, J. M.; Daniels, A. D.; Kudin, K. N.; Strain, M. C.; Farkas, O.; Tomasi, J.; Barone, V.; Cossi, M.; Cammi, R.; Mennucci, B.; Pomelli, C.; Adamo, C.; Clifford, S.; Ochterski, J.; Petersson, G. A.; Ayala, P. Y.; Cui, Q.; Morokuma, K.; Malick, D. K.; Rabuck, A. D.; Raghavachari, K.; Foresman, J. B.; Cioslowski, J.; Ortiz, J. V.; Baboul, A. G.; Stefanov, B. B.; Liu, G.; Liashenko, A.; Piskorz, P.; Komaromi, I.; Gomperts, R.; Martin, R. L.; Fox, D. J.; Keith, T.; Al-Laham, M. A.; Peng, C. Y.; Nanayakkara, A.; Gonzalez, C.; Challacombe, M.; Gill, P. M. W.; Johnson, B.; Chen, W.; Wong, M. W.; Andres, J. L.; Gonzalez, C.; Head-Gordon, M.; Replogle, E. S.; Pople, J. A. Gaussian 98, Revision A.7; Gaussian, Inc.: Pittsburgh, PA, 1998.
(47) McMillen, D. F.; Barker, J. R.; Lewis, K. E.; Trevor, P. L.; Golden, D. M. "SRI Project PYU-5787,", 1979.
(48) Maksimov, Y. Y.; Apol'kova, V. N.; Braverman, O. V.; Solov'en, A. I. *Russ. J. Phys. Chem.* **1985**, *59*.
(49) Burov, Y. M.; Nazin, G. M. *Kinet. Catal.* **1982**, *23*, 5.
(50) Belyayeva, M. S.; Klimenko, G. K.; Babaytseva, L. T.; Stolyarov, P. N. Fifth All Union Symposium on Combustion and Detonation, 1977.
(51) Reid, R. C.; Prausnitz, J. M.; Sherwood, T. K. *The Properties of Gases and Liquids: Their Estimation and Correction*; McGraw-Hill: New York, 1977.